Acta Physica Hungarica 62 (2—4), pp. 321—346 (1987)

UNUSUAL MAPS AND THEIR USE TO APPROACH USUAL ONES*

Z. KAUFMANN

Institute for Solid State Physics, Roland Eötvös University
1088 Budapest, Hungary

P. SZÉPFALUSY

Institute for Solid State Physics, Roland Eötvös University
1088 Budapest, Hungary

and

Central Research Institute for Physics
1525 Budapest, Hungary

and

T. TÉL

Institute for Theoretical Physics, Roland Eötvös University
1088 Budapest, Hungary

One-dimensional maps coupled to discrete valued variables are introduced. They are designed to describe the motion in Lorenz and Hénon type systems on branched manifolds arising by expanding the maps in powers of the inverse dissipation strength, or by coarse graining. The maps are studied in detail along the crisis line where they exhibit complex behaviour with periodic and chaotic attractors. The convergence to the Hénon map is investigated numerically and found to be satisfactory for not too weak dissipations.

1. Introduction and summary

Our view concerning mechanical and other types of motion has drastically changed owing to recent developments in the theory of dynamical systems [1–3]. It is nowadays clear that the long-time behaviour of deterministic nonlinear systems with at least one and a half degrees of freedom generically exhibits unpredictable, chaotic motion in a certain region. Since this type of motion has stochastic features its complete description requires statistical methods [1–3].

Following an idea of Poincaré [4] it is often convenient to consider a discrete dynamics, a mapping generated by either the intersection points of the continuous trajectories with a certain surface of the phase space (Poincaré map) or by taking subsequent snapshots of the motion with a given periodicity (stroboscopic maps). The form of the mapping follows uniquely from the continuous motion, the inverse is,

* Dedicated to Prof. K. Nagy on his 60th birthday

however, not true, the same map can belong to several systems. General properties of chaotic motions are most commonly studied by investigating maps exhibiting chaotic behaviour [1–3, 5, 6].

Besides general common features, there are certain differences in the chaotic behaviour of conservative (Hamiltonian) and dissipative systems. In the former case, the fact whether a trajectory is chaotic depends strongly on its initial conditions. Chaotic trajectories then wander in a region of phase space the volume of which is nonzero [1, 2, 7]. In dissipative systems practically all trajectories are attracted towards a zero volume object, the attractor, of the phase space. Chaotic attractors, are strange sets [1–3, 8] characterized by noninteger, or fractal dimensions [9]. In this paper we shall be interested in dissipative systems which show up, besides mechanical phenomena, in the theory of nonequilibrium systems exhibiting instabilities leading to a new, turbulent macroscopic state.

In the simplest cases the associated Poincaré or stroboscopic map describes a dynamics of two variables, and the chaotic attractor has a dimensionality between 1 and 2. We derive the most essential features of the map in two important classes of systems, namely in systems where trajectories do not pass close to a singular point, and in systems where they do pass close to a hyperbolic point. The first class contains among many well-known examples the Rössler model [10] and the periodically kicked harmonic oscillator, where even an exact derivation of the map is possible. The maps generated in this class possess analytic forms and a smoothly position dependent area contracting ratio, the Jacobian of the map, which can be considered to be constant near the attractors. This type of maps will be called Hénon type one since Hénon's famous map [11, 12] belongs to this family. A standard example of the second class is the Lorenz model [13], but the Rikitake dynamo [14] and another model of Rössler [15] are also of this type. (For a discussion of general properties of the flow see [16]). The corresponding maps, called Lorenz type maps, are characterized by a singular form and a strongly position dependent Jacobian which vanishes or diverges along a certain line of the plane. The singularities are described by power laws the exponent of which is given by the ratios of the eigenvalues of the linearized equation of motion around the hyperbolic fixed point [17–21].

The asymptotic behaviour in dissipative chaotic systems is described by means of a stationary distribution concentrated on the chaotic attractor. Unfortunately, little is known about the existence and the properties of such distributions for maps of the plane. The situation simplifies considerably in the limiting case of an extremely small Jacobian, which, however, occurs quite often as a consequence of a strong dissipation in the continuous system or of rather long periods of shapshots or of turnover times.

In Hénon type cases the map typically reduces in this limit to a map of the interval defined by a continuous single humped function. Parameter settings when the maximum is mapped in two steps into an unstable fixed point, are of importance, since the chaotic character of the motion may then be shown with mathematical rigor. An essential condition for the existence of a unique stable stationary distribution in this

situation is the negativity of the so-called Schwarzian derivative of the map [5, 6]. In common cases this condition is fulfilled automatically.

If at the above-mentioned parameter setting the map generates chaotic trajectories the case of fully developed chaos [22] is realized. This is, at the same time, a crisis configuration [23] since an unstable orbit collides with the chaotic attractor. Crisis is, however, not restricted to chaotic attractors. It is rather a configuration on a capture/escape boundary [24].

Reduced Lorenz type maps obtained in the limit of vanishing Jacobian are more complicated. Firstly, the dynamics which is still a map of the interval, turns out to have a one-step memory since the state of the system depends also on the sign of the preimage of the variable [21]. Secondly, if a certain internal symmetry is maintained, the memory can be transformed out but the resulting 1D map is not obviously a single-humped one, and its Schwarzian derivative can be also positive. Our numerical simulations show that crisis situations in these cases do not necessarily imply chaos: chaotic regions are interrupted by periodic windows when changing a parameter of the map by keeping its maximum mapped in two steps into an unstable fixed point. In a special case when the effect of a positive Schwarzian derivative has been amplified by making the map discontinuous we were able to find even an asymptotic analytic formula specifying the position of such periodic windows.

Furthermore, we investigated maps with strong but finite dissipation. A perturbative expansion is worked out for the dynamics based on the method of [25] designed originally to determine the shape of chaotic attractors. In a first order calculation in Lorenz type maps we obtain a dynamics with a two-step memory expressed through the presence of the sign of two subsequent preimages as additional discrete variables. In symmetric systems this map can be reduced to a dynamics with a single additional discrete variable. We show that such a dynamics characterizes also the first order approximation of Hénon type maps. In higher order calculations the dynamics will have more and more discrete variables and the attractor will be approximated by a larger and larger number of branches. Finally, this attractor is hard to be distinguished from the chaotic attractor appearing in the map of the plane but using a finite resolution. In this sense unusual maps of an interval with several additional discrete variables, which can also be considered as 1D maps with several discontinuities, may be useful approximations of mappings of the plane. In higher orders, however, to carry out the calculation requires rapidly increasing numerical efforts. Instead, we have followed here an approach in the same spirit but technically easier to handle. Namely, we have considered a discretized approximation of the Hénon map in which one of the recursions is replaced by a step function with several steps, leaving the other recursion unchanged. The condition for crisis and the position and structure of a few periodic cycles have been compared in approximate and exact maps and a satisfactory agreement has been found at step numbers as low as 20–40, illustrating that the discretized version can be a reasonable approximate dynamics.

The paper is organized as follows. Sections 2 and 3 contain the derivation of Hénon and Lorenz type maps, respectively. Section 4 is devoted to the study of reduced symmetric Lorenz type maps in the limit of extremely strong dissipation. Emphasis is laid on a discontinuous version in which periodic windows of the map in crises are analytically specified. The characterization of certain satellite windows is given in the Appendix. In Section 5 the perturbative method valid in the case of strong but finite dissipation is applied for determining approximate dynamics. Finally in Section 6 we study a discretized Hénon map and compare certain properties of it with those of the exact Hénon map.

2. Hénon type maps

The relation between a flow and the associated discrete dynamics can be conveniently studied in periodically kicked systems. For kick lengths negligible on the time scale of the macroscopic motion, the succession of kicks is described by a periodic Dirac delta term in the equation of motion. The effect of a kick is then a jump in the momentum. If the evolution of the system is known between subsequent kicks, an exact form follows for the stroboscopic map.

The map

We consider here the linearly damped one-dimensional harmonic oscillator under the influence of periodic Dirac delta kicks the amplitude of which is position dependent in a nonlinear way. Let T denote the period of the kicks and let $\bar{f}(x)$ represent the velocity jump caused by a kick acting at an actual position coordinate x. The form of $\bar{f}(x)$ is arbitrary. By means of the well-known solution of a damped oscillator of eigenfrequency ω_0 and friction coefficient 2γ one obtains for the stroboscopic map (see e.g. [1])

$$x' = xE\left(C + \frac{\gamma}{\omega}S\right) + v\frac{E}{\omega}S,$$
$$v' = vE\left(C - \frac{\gamma}{\omega}S\right) - xE\frac{\omega_0^2}{\omega}S + \bar{f}(x'), \tag{2.1}$$

where x, v denote position and velocity after the nth kick and the following abbreviations have been used

$$\omega = (\omega_0^2 - \gamma^2)^{1/2},$$
$$C = \cos\omega T, \quad S = \sin\omega T, \quad E = \exp(-\gamma T). \tag{2.2}$$

For a general $\bar{f}(x)$ (2.1) is a nonlinear map of the x, v plane. Its form simplifies considerably by introducing another position type coordinate y defined by

$$y = x\frac{1}{E}\left(C - \frac{\gamma}{\omega}S\right) - v\frac{S}{E\omega} + \bar{f}(x)\frac{S}{E\omega}. \tag{2.3}$$

This leads to

$$x' = 2ECx + \frac{ES}{\omega} f(x) - E^2 y,$$

$$y' = x. \tag{2.4}$$

Note that the Jacobian of this map is E^2, in accordance with the fact that the amplitude of the oscillator decreases in an interval of length T by a factor $\exp(-\gamma T)$. After introducing

$$f(x) \equiv 2ECx + \frac{ES}{\omega} f(x), \qquad b \equiv -E^2, \tag{2.5}$$

(2.4) can be rewritten in the form

$$x' = f(x) + by,$$

$$y' = x. \tag{2.6}$$

We call the map (2.6) of Hénon type since for

$$f(x) = 1 - ax^2 \tag{2.7}$$

(in dimensionless units) Hénon's map [11, 12] is recovered, which is known to be the most general quadratic map of the plane with a constant Jacobian. For $f(x) = 1 - a|x|$ (2.6) is the Lozi map [26]. As illustrated by these examples, Hénon type maps often describe chaotic (at least in a numerical sense) behaviour and possess for $|b| < 1$ chaotic attractor in the x, y plane.

The fact that there are no singular points in the phase space of the kicked damped harmonic oscillator turns out to be a crucial property. In all systems the trajectories of which do not pass close to a singular point around the attractor the associated map of the plane, describing the motion on or near the attractor, is expected to be Hénon's map since it must then be analytic in x and y. As an example we mention the Rössler model at its standard parameter values [10, 27], the Poincaré map of which is really of the form of (2.6), (2.7).

The limit of extremely strong dissipation

Strong dissipation means that the Jacobian of the map is tending toward zero. In the limit $b \to 0$ (2.6) becomes a one-dimensional map

$$x' = f(x), \tag{2.8}$$

since y is then a dummy variable. Such maps of the interval have been extensively studied in the literature from both of the point of view of the bifurcation sequence [28, 29, 6], of universal features [30, 31] and of the properties of the chaotic state [5, 6, 22]. We shall use this type of maps as a point of reference when investigating more general cases.

3. Lorenz type maps

In cases when trajectories on or near the attractor pass close to saddle points the corresponding Poincaré map drastically differs from (2.6). The reason is that a saddle point has at least one invariant hypersurface on which it is attracting. Therefore, trajectories approaching this hypersurface may stay for arbitrarily long time in the vicinity of the saddle and cause singularities in the form of the Poincaré map (Shilnikov's method [32]). As a consequence, the Jacobian of the map will be strongly position-dependent. The standard example of such systems is the Lorenz model [13] where the origin is a hyperbolic point belonging to the Lorenz attractor. General systems with this type of singularity on the attractor, and having no other singularities, we shall call Lorenz type and the corresponding Poincaré map Lorenz type map. Different approximate forms for this map have been deduced by using basically Shilnikov's method [17–21], among which that of [21] seems to be the most general one. It is worth mentioning that systems with a saddle type focus point have also been studied [33–36] and possess singular maps but different from Lorenz type.

The map

For sake of completeness we outline the derivation of the map and refer for the details to [21].

A three-dimensional dynamical system is considered with variables X_i, $i=1, 2, 3$ the time evolution of which is governed by autonomous ordinary differential equations. Let the origin of the phase space X_1, X_2, X_3 be a hyperbolic point with a two-dimensional stable manifold and a one-dimensional unstable manifold, $W^u(0)$ like in the Lorenz model. For simplicity, the variables X_i are chosen to be the normal modes of the linearized equations around the origin with eigenvalues λ_i, so that X_1 belongs to the unstable mode, i.e. $\lambda_1 > 0$ but $\lambda_2 < \lambda_3 < 0$.

The Poincaré surface is chosen as the $X_3 = z = \text{const}$ plane where z is adjusted in such a way that the unstable manifold of the hyperbolic point should intersect the plane. In a certain reference frame on this plane the coordinates are denoted by x, y. We use the convention that only intersections from above belong to the map. The points D^+ and D^- will be of special importance, where $D^+(D^-)$ represents the first intersection point between the $X_3 = z$ plane and that branch of the unstable manifold $W^u(0)$ which emanates into the positive (negative) X_1 direction (Fig. 1).

Since the plane $X_3 = z$ is generally outside the region where the motion can be well approximated by the linearized equations around the hyperbolic fixed point, we introduce an auxiliary surface defined by $X_3 = Z$, where Z is a sufficiently small constant. The reference frame X, Y on this surface is chosen in such a way that the origin $X = Y = 0$ is the intersection point of the plane and the X_3 axis, and the $X(Y)$ axis is parallel with the $X_1(X_2)$ axis.

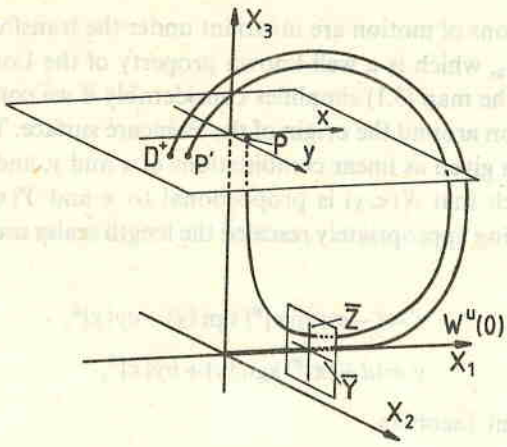

Fig. 1. The unstable manifold $W^u(0)$ and a trajectory passing close to the hyperbolic point in Lorenz type systems

Trajectories passing close to the hyperbolic point must start from the neighbourhood of the stable manifold. The trajectory emanated from $P=(x, y)$ crosses the $X_3=Z$ plane at a certain point (X, Y). More generally, the flow generates a map $X=X(x, y)$, $Y=Y(x, y)$ between the two surfaces, where $X(x, y)$ and $Y(x, y)$ are smooth functions of their variables since no singular point lies between the planes $X_3=z$ and $X_3=Z$. An appropriate choice for Z always guarantees that both coordinates X, Y of the intersection with the auxilary plane will be small. The subsequent motion of the point $(X(x, y), Y(x, y), Z)$ is thus described by the solution of the linearized equations around the origin.

As, after having left the hyperbolic point, the trajectory does not pass near any singular point, the deviation between the next intersection $P'=(x', y')$ with the Poincaré surface and $D^+(D^-)$, if $X(x, y)>0$ (if $X(x, y)<0$), is an analytic function of the coordinates $\bar{Y}$ and $\bar{Z}$ (Fig. 1). For small values of X and Y it is sufficient to keep the first terms of the Taylor expansion only, apart from exceptional cases when their coefficients vanish. Finally, one finds [21] as a typical form of the map near $X(x, y)=0$

$$x'=(u+a_{11}|X(x, y)|^{\beta})\,\mathrm{sgn}\,(X(x, y))+a_{12}Y(x, y)|X(x, y)|^{\delta},$$
$$y'=(v+a_{21}|X(x, y)|^{\beta})\,\mathrm{sgn}\,(X(x, y))+a_{22}Y(x, y)|X(x, y)|^{\delta}, \qquad (3.1)$$

where

$$\beta=|\lambda_3|/\lambda_1, \qquad \delta=|\lambda_2|/\lambda_1, \qquad (3.2)$$

$\mathrm{sgn}\,(X)$ denotes the sign of X, the coefficients a_{ij} are constants, and u, v are the coordinates of the point D^+. For the sake of simplicity we assumed by writing down

(3.1) that the equations of motion are invariant under the transformation $X_1 \to -X_1$, $X_2 \to -X_2$, $X_3 \to X_3$, which is a well-known property of the Lorenz model.

The form of the map (3.1) simplifies considerably if we consider the recursions only in a small region around the origin of the Poincaré surface. The functions $X(x, y)$ and $Y(x, y)$ are then given as linear combinations of x and y, and we may choose the reference frame such that $X(x, y)$ is proportional to x and $Y(x, y)$ to y in the new variables. After having appropriately rescaled the length scales used in both directions, one arrives at

$$x' = (-e + a|x|^{\beta}) \operatorname{sgn}(x) + cy|x|^{\delta},$$
$$y' = (d + |x|^{\beta}) \operatorname{sgn}(x) + by|x|^{\delta}, \tag{3.3}$$

with an x-dependent Jacobian

$$J(x) = (ab - c)\beta|x|^{\eta}, \tag{3.4}$$

where $\eta = \beta + \delta - 1$. In the following $a, b, e > 0$, $ab \geq c$ will be assumed.

The general form of the Poincaré map contains, of course, additional terms, analytic or less singular as those given already by Eq. (3.3). In order to illustrate the consequences of the singular feature of the map, however, it is sufficient to keep the most singular part. Therefore, we consider in the following the map obtained by extending the validity of equation (3.3) to the whole plane. More precisely, we regard the map (3.3) as a model which is designed to simulate some essential features of Lorenz type systems. In numerical simulations the map was found to possess a chaotic attractor at several values of the parameters [21] (as an example see Fig. 2).

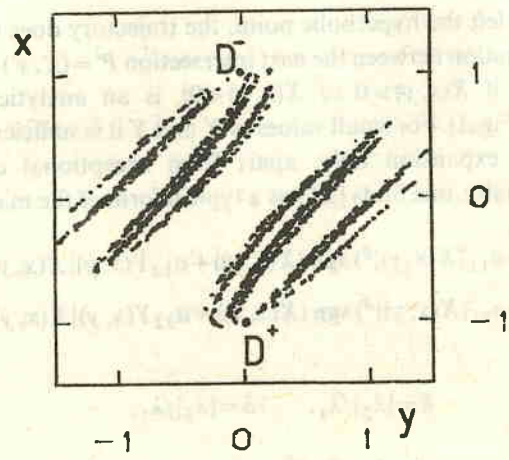

Fig. 2. The chaotic attractor of the map (3.3) obtained in a numerical simulation after 2000 steps. The parameters are $a = 1.5$, $b = 0.7$, $c = 0.25$, $d = 0$, $e = 1$, $\beta = 0.6$, $\delta = 0.2$

The limit of extremely strong dissipation

The limiting case of an identically vanishing Jacobian is realized if the parameters fulfil the relation $c=ab$. It follows then from (3.3) that any starting point jumps immediately on one of the straight lines $x=ay\mp(e+ad)$ where the attractor is situated. The sign $+(-)$ is to be taken if the point (x, y) is on the lower (upper) branch. Once, however, a point is on the lower (upper) branch, the x-coordinate of its preimage has to be positive (negative). Thus, the sign before the parenthesis is identical with that of the preimage of x.

Using this relation between x and y as well as (3.3) x' can be expressed in terms of x. We obtain

$$x'=\operatorname{sgn}(x)\,(-e+a f_{\sigma\operatorname{sgn}(x)}(|x|)), \tag{3.5}$$

where

$$f_{\pm}(|x|)=|x|^{\beta}+\frac{b}{a}(|x|\pm(e+ad))|x|^{\delta} \tag{3.6}$$

and σ denotes the sign of the preimage of x. The y' coordinate is then determined by x' through

$$y'-\operatorname{sgn}(x)d=(x'+\operatorname{sgn}(x)e)/a. \tag{3.7}$$

The special two-step nature of the dynamics can be made clearer by rewriting (3.5) as

$$\begin{aligned} x' &= (-e+a|x|^{\beta})\operatorname{sgn}(x)+bx|x|^{\delta}+g\sigma|x|^{\delta}, \\ \sigma' &= \operatorname{sgn}(x), \end{aligned} \tag{3.8}$$

where $g=b(e+ad)$. Considering (3.8) as a map of the interval, it can be specified by the functions $f_{\pm}(x)$ given in (3.6) and by the rule that $f_{+}(f_{-})$ is to be taken if $\sigma\operatorname{sgn}(x)$ is positive (negative) (see [21] where also plots of $f_{\pm}$ are given). Without any internal symmetry, a two-step dynamics cannot be simplified further.

Owing, however, to the symmetry property mentioned after (3.2), the form of the map may be reduced. By introducing $p=-\sigma x$ as a new variable branches of $f_{\pm}$ pairwise coincide. This procedure is similar in spirit to Lanford's treatment of the Lorenz model [37]. The recursion for p is then obtained as

$$p'=h(p)\equiv e-a|p|^{\beta}-b|p|^{1+\delta}+g\operatorname{sgn}(p)\,|p|^{\delta}, \tag{3.9}$$

which is characterized by a single-valued continuous (but asymmetric) function, h.

The representation (3.9) is well suited for discussing the basic questions of the existence of a unique stationary probability distribution with a density since this problem has extensively been studied in the case of such continuous 1D maps.

Four cases should be distinguished: a) $\beta<\delta$, $\beta<1$ (like in the standard Lorenz model); b) $\beta<\delta$, $\beta>1$; c) $\beta>\delta$, $\delta>1$; d) $\beta>\delta$, $\delta<1$ (Fig. 3). In case a) the map has a cusp,

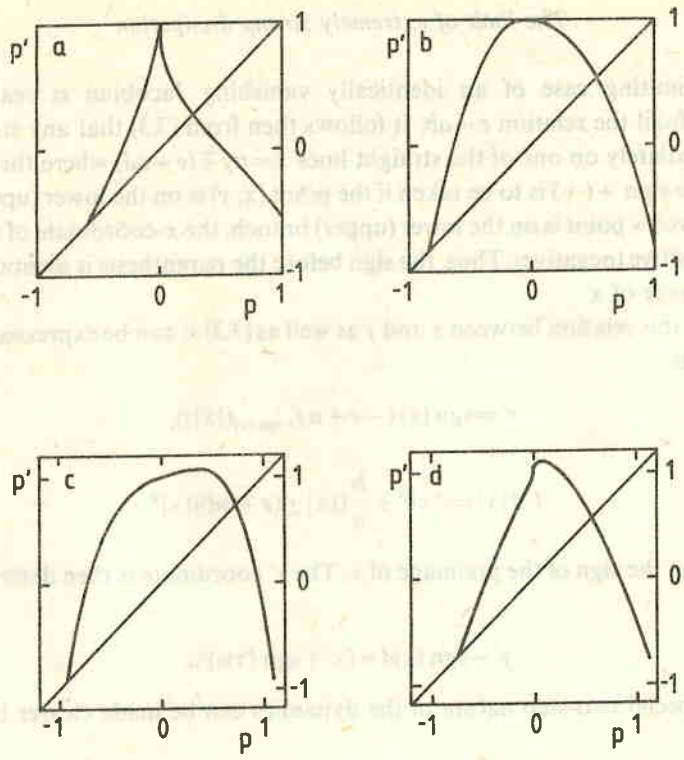

Fig. 3. Qualitatively different shapes of $p' = h(p)$ (3.9) obtained at different choices of the exponents β and δ. The parameters a, b are adjusted in such a way that the maximum is mapped in two steps into the negative fixed point; $e = 1$, $d = 0$ everywhere.
Case a): $\beta = 0.5$, $\delta = 1.5$, $a = 1.560$, $b = 0.6$,
Case b): $\beta = 2$, $\delta = 3$, $a = 1.839$, $b = 0.5$,
Case c): $\beta = 4$, $\delta = 1.2$, $a = 1.430$, $b = 0.5$,
Case d): $\beta = 1.5$, $\delta = 0.5$, $a = 1.491$, $b = 0.5$.
(Numerically all cases seem to be chaotic at these values)

while in cases b), c) and d) it has a smooth maximum (at certain special choices of the parameters two or three local maxima may be present). In the former case, if the map is everywhere expanding, well-known theorems apply and the existence of the unique probability density is ensured (see [5, 6] and references therein). In the latter cases the map can produce chaotic iterations for typical initial conditions only at particular control parameter values. The situation when the maximum point is mapped in two steps to an unstable fixed point, i.e., when fully developed chaos can exist, has been most extensively studied. Two basic conditions under which the existence of a unique absolutely continuous invariant measure has been proved in this situation are that the first derivative of the map is nonzero except at the maximum and that its Schwarzian derivative is negative [5, 6]. Both can be valid in case b), but in cases c) and d) the first and the second condition is violated near $x = 0$, respectively.

4. A discontinuous limiting case of Lorenz type maps

Our aim is here to investigate in some detail the characteristic features of maps belonging to case *d*. In the limit of strong dissipation — as it was pointed out in the previous section — the one-dimensional map $p' = h(p)$ as given by (3.9) has a positive Schwarzian derivate around $p = 0$. In order to study the consequences of this property we turn to the extreme case of $\delta = 0$ where the rapidly changing part of $h(p)$ around $p = 0$ is replaced by a jump. After setting $e = 1$ and choosing, as a typical value, $\beta = 2$, the map still has three independent parameters: a defining the quadratic part, b giving the modulus of the slope at $p = 0$, and g characterizing the jump there. For a sufficiently large value of b the map can be everywhere expanding. An interesting interplay between periodic and chaotic behaviour is, therefore, expected to be present for small b-s. The phenomena found at $b \ll 1$ are qualitatively similar to those at $b = 0$, thus in the following we consider the map

$$p' = h(p) \equiv 1 - ap^2 + g \operatorname{sgn}(p). \tag{4.1}$$

We restrict our attention to the region $0.8 < a \leq 2$, $0 \leq g \leq 1$. The plot of $h(p)$ is displayed in Fig. 4. (4.1) is a straightforward extension of the parabola map $p' = 1 - ap^2$ which is recovered as a special case for $g = 0$.

The situation when the maximum point of a single humped continuous map is mapped in two steps to an unstable fixed point is of importance since fully developed chaos [22] may then exist. This corresponds, at the same time, to a crisis situation [23] since an unstable orbit collides with the chaotic attractor. Such a crisis configuration may also be found in (4.1) with an appropriate choice of the parameters a and g but, as we shall see, it does not necessarily imply chaos.

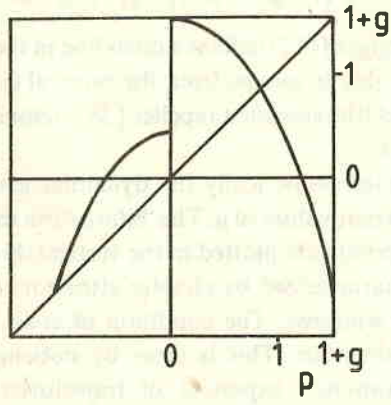

Fig. 4. Plot of the function $h(p)$ defining (4.1). A crisis situation is shown at $a = 1.140$, $g = 0.556$

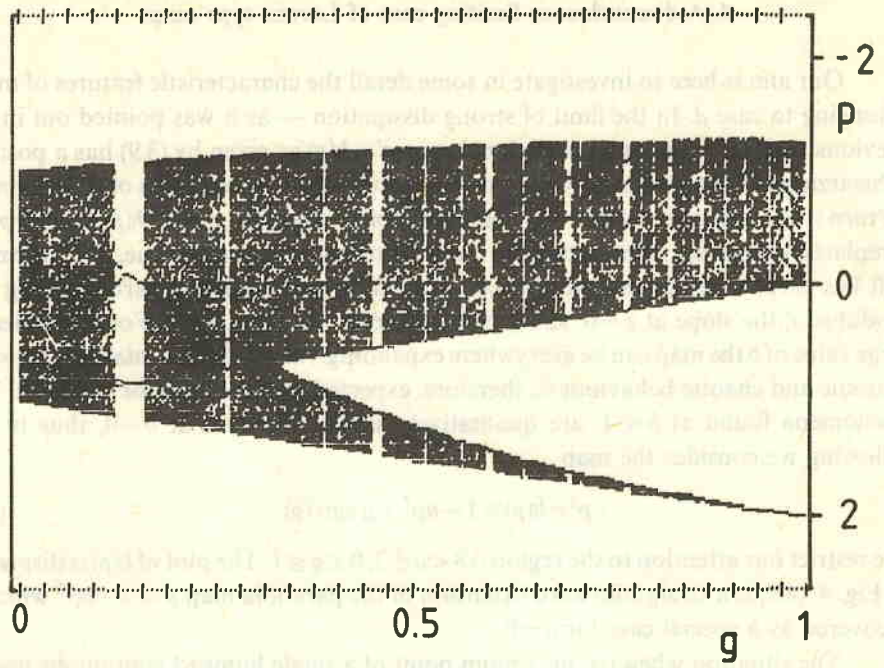

Fig. 5. Bifurcation diagram along the crisis line of (4.1) in the region $0 \leq g \leq 1$. A regular sequence of relatively broad periodic windows can be seen

The maximum point $h(+0)=1+g$ is mapped into the fixed point $p^*=-(1+\sqrt{1+4a(1-g)})/(2a)$ if the relation

$$a^3(1+g)^4-2a^2(1+g)^3+2g=0 \tag{4.2}$$

is fulfilled. The solution $a_c(g)$ of (4.2) defines a crisis line in the parameter plane a, g. For $a>a_c(g)$ trajectories are able to escape from the interval $(p^*, 1+g)$. Only trajectories belonging to a Cantor set (the so-called repeller [38]) remain then bounded, provided no attracting cycle exists.

We have investigated numerically the dynamics generated by (4.1) along the crisis line $a=a_c(g)$ at different values of g. The 'bifurcation diagram' of Fig. 5 shows the results, where attractor points are plotted in the vertical direction. It is clear from this diagram that regions characterized by chaotic attractors (in a numerical sense) are interrupted by periodic windows. The condition of crisis is for maps like (4.1) not sufficient for chaotic behaviour. This is clear by noticing that the large negative contribution to the Lyapunov exponent of trajectories starting from the right neighbourhood of the origin is compensated by staying for a long time around the unstable fixed point, but this is no longer true for trajectories starting from the left neighbourhood of $p=0$, which may, thus, produce a negative Lyapunov exponent at certain values of g, along the crisis line.

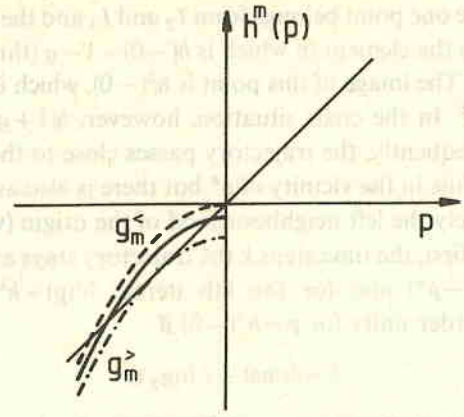

Fig. 6. The shape of the mth iterate of $h(p)$ in a left neighbourhood of the origin (bold line) for $g_m^< < g < g_m^>$

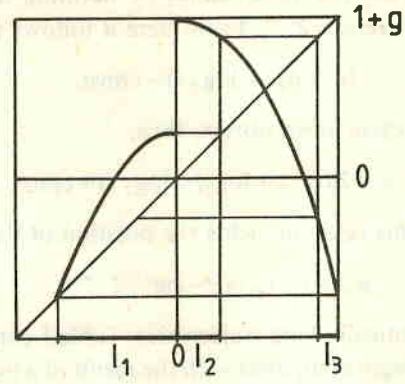

Fig. 7. The action of the map (4.1) on the interval I_1 in crisis configuration

There is a striking regularity in the sequence of periodic windows for $g \to 1$ (Fig. 5). In the following we study how to specify these windows. First, it is to be noted that the mth iterate of $h(p)$, the stable fixed point of which is an element of the period-m cycle of the original map, has the shape sketched in Fig. 6 in the vicinity of the origin. When increasing g the left branch of $h^m(p)$ is shifted downwards and at a certain value $g_m^<$ (dashed line) $h^m(-0)$ reaches the origin. Then a stable fixed point, and by that a stable limit cycle appears. By increasing g further, it exists till a certain $g_m^>$, the stable and unstable fixed points of h^m coincide. The m-cycle disappears at $g_m^>$ via a tangent bifurcation (dashed dotted line).

Next, we specify the position of the periodic windows. For $g > g_3^<$ the intervals I_1, I_2, I_3 shown in Fig. 7 are mapped as follows:

$$I_1 \to I_1 + I_2, \qquad I_2 \to I_3, \qquad I_3 \to I_1. \tag{4.3}$$

To every periodic cycle one point belongs from I_2 and I_3 and the rest of points from I_1. Let us consider a cycle the element of which is $h(-0)=1-g$ (this is the case at $g=g_m$). For $g\to 1$ $1-g\equiv\varepsilon\ll 1$. The image of this point is $h^2(-0)$, which is mapped into $h^3(-0)=h(1+g)-h'(2-\varepsilon)a\varepsilon^2$. In the crisis situation, however, $h(1+g)=p^*$, thus $h^3(-0)=p^*-h'(2-\varepsilon)a\varepsilon^2$. Consequently, the trajectory passes close to the unstable fixed point p^*. It will stay for a while in the vicinity of p^* but there is also another region where it will be captured, namely the left neighbourhood of the origin (where the map is flat).

Let us estimate first, the time steps k the trajectory stays around p^*. Since $f'(p^*)=2$, $h(p)-h(p^*)\cong 2(p-p^*)$ and for the kth iterate $h^k(p)-h^k(p^*)\cong 2^k(p-p^*)$. This difference will be of order unity for $p=h^3(-0)$ if

$$k=\text{const}-2\log_2\varepsilon. \tag{4.4}$$

The trajectory must return to $p=-0$. Therefore, after leaving the vicinity of p^* it must reach a point $\bar{p}$ for which $h^l(\bar{p})=-0$. Since the map is $h(p)=\varepsilon-ap^2$ for $p<0$, $h^{l-1}(\bar{p})=-(\varepsilon/a)^{1/2}$ holds. On the other hand, by iterating forward $p=\bar{p}$ one finds $h^{l-1}(\bar{p})=-(a|\bar{p}|)^{\omega}a^{-1}$, where $\omega=2^{l-1}$. From here it follows that

$$l=\log_2(-\log_2\varepsilon)+\text{const}. \tag{4.5}$$

For the total length of a cycle m we obtain, thus,

$$m=-2\log_2\varepsilon+\log_2(-\log_2\varepsilon)+\text{const}. \tag{4.6}$$

for $\varepsilon\to 0$. The inverse of this relation yields the position of the m-cycle at

$$g_m^{<}=1-\varepsilon_m=1-cm^{1/2}2^{-m/2} \tag{4.7}$$

which is valid for asymptotically long trajectories. Table I contains this approximate value for cycles of finite length compared with the result of a numerical solution of $g_m^{<}$.

These considerations show that there is an infinite sequence of periodic windows in the map (4.1) when changing the parameters in such a way that the condition for crisis (4.2) is maintained. Note that there is a geometric sequence of periodic windows also in the parabola map for $a\to 2$ [31], however, in a pre-crisis situation. The sequence described by (4.7) is of quite different nature. The presence of the prefactor $m^{1/2}$ is a consequence of the smooth local maximum of the map at $p=-0$ while the exponent $-m/2$ follows from the fact that the map is discontinuous at the origin. It is worth mentioning the result obtained for an arbitrary exponent $\beta>1$, i.e. for the map $h(p)=1-a|p|^{\beta}+g\,\text{sgn}(p)$. The same argumentation then yields

$$g_m^{<}=1-cm^{\rho}(h'(p^*))^{-m/\beta} \tag{4.8}$$

with

$$\rho=\frac{\log_2 h'(p^*)}{\beta\log_2\beta}. \tag{4.9}$$

Table I

Stable periodic orbits in (4.1) along its crisis line. m denotes the length of the periodic orbit, g_m is the control parameter value where it appears by increasing g. The third column contains the results of the formula (4.7) with the fitted value $c = 1.05$. Numbers in the last column yield a measure of the accuracy of (4.7)

m	$g^<$	$1-1.05(m2^{-m})^{1/2}$	$\frac{1.05(m2^{-m})^{1/2}}{1-g^<}$
3	0.452875	0.357009	1.175
4	0.593984	0.475000	1.293
5	0.696769	0.584951	1.368
6	0.771194	0.678504	1.405
7	0.826018	0.754454	1.411
8	0.867098	0.814384	1.396
9	0.898288	0.860788	1.368
10	0.922182	0.896238	1.333
11	0.940582	0.923048	1.295
12	0.954777	0.943167	1.256
13	0.965722	0.958172	1.220
14	0.974137	0.969307	1.186
15	0.980580	0.977535	1.156
16	0.985489	0.983594	1.130
17	0.989207	0.988042	1.107
18	0.992008	0.991299	1.088
19	0.994105	0.993679	1.072
20	0.995668	0.995414	1.058
21	0.996827	0.996677	1.047
22	0.997682	0.997595	1.037
23	0.998311	0.998261	1.029
24	0.998772	0.998744	1.022
25	0.999109	0.999094	1.016
26	0.999354	0.999346	1.011
27	0.999533	0.999529	1.008
28	0.999663	0.999661	1.005
29	0.999757	0.999756	1.003
30	0.999824	0.999824	0.9982

Since, however, for $g \to 1$ the fixed point is $p^* = -a^{-\frac{1}{\beta-1}}$, $h'(p^*) = \beta$ and, thus

$$g_m^< = 1 - cm^{1/\beta}\beta^{-m/\beta} \tag{4.10}$$

follows for the position of the m-cycle.

Satellite series of windows approaching $g_m^<$ and $g_m^>$ can also be specified. A detailed description of them is given in the Appendix by means of itinerary sequences.

Finally, it is worth emphasizing that an interplay between chaotic and periodic regions along the crisis line is characteristic not only for the map (4.1) but also for certain subclasses of (3.9). Namely, the same phenomenon can be found in maps with $\delta \ll 1$ and $\beta > 1$ and also in maps where $h(p)$ possesses two points with a vanishing first derivative (case c).

5. Discrete dynamics on branched manifolds

Chaotic attractors of systems with finite dissipation consist of infinitely many branches arranged in a fractal structure. If, however, the dissipation is strong only a few branches can be observed owing to the limited accuracy of the measurement. It may then be convenient to consider these branches to be infinitely narrow. They are called branched manifolds [16]. The dynamics on such branched manifolds is, of course, noninvertible since several original branches are considered as identical. Our aim is here to specify branched manifolds of Lorenz and Hénon type maps and to determine the dynamics on them. We shall apply the perturbative method worked out in [25] which determines the shape of the attractor as a power series in the inverse dissipation strength. The dynamics will turn out to be a map of the interval which depends, however, also on certain discrete variables, in lowest orders on the sign of subsequent preimages of the continuous variable.

Lorenz type maps

We start to investigate this type of maps since here even in the limit of extremely strong dissipation a dynamics with a special two-step nature has been found (cf. (3.8)). The deviation from this limiting case is measured now by

$$\varepsilon = ab - c, \tag{5.1}$$

a factor of the Jacobian (3.4). From (3.3) it follows that

$$x' - ay' + \operatorname{sgn}(x) g/b = -\varepsilon y |x|^{\delta}. \tag{5.2}$$

In a first order calculation in ε, it is sufficient to use the 0th order result (3.5) and (3.7) on the right hand side. Thus, we obtain for the shape of the attractor

$$x = ay - \sigma g/b - \frac{\varepsilon}{a}\left(\sigma f_{\sigma\tau}^{-1}(y\sigma - d) + \tau g/b\right)\left(f_{\sigma\tau}^{-1}(y\sigma - d)\right)^{\delta}, \tag{5.3}$$

where $f_{\pm}^{-1}$ denotes the inverse of $f_{\pm}$ defined in (3.6) and σ and τ stand for the sign of the first and second preimage of x, respectively. An elimination of y from the first equation of (3.3) by means of (5.3) yields the dynamics of the x-variable as

$$\begin{aligned} x' = {} & (-e + a|x|^{\beta}) \operatorname{sgn}(x) + bx|x|^{\delta} + \sigma g |x|^{\delta} + \\ & + \frac{\varepsilon}{a}|x|^{\delta}\left[-x - \sigma g/b + \left(\sigma f_{\sigma\tau}^{-1}\left(\frac{e + x\sigma}{a}\right) + \tau(e + ad)\right)\right]\left(f_{\sigma\tau}^{-1}\left(\frac{e + x\sigma}{a}\right)\right)^{\delta}, \\ \sigma' = {} & \operatorname{sgn}(x), \\ \tau' = {} & \sigma. \end{aligned} \tag{5.4}$$

Note that both the shape and the dynamics depend on two discrete variables σ and τ, and that for extremely strong dissipation, $\varepsilon = 0$, the dependence on the second preimage disappears.

Since the map (3.3) is inversion symmetric, the memory of the dynamics (5.4) can be reduced by introducing again, like in Section 3, $p = -\sigma x$ as a new variable. In this representation (5.4) has the form

$$p' = e - a|p|^{\beta} - b|p|^{1+\delta} + g\,\mathrm{sgn}\,(p)\,|p|^{\delta} +$$
$$+ \frac{\varepsilon}{a}|p|^{\delta}\left\{|p| + \mathrm{sgn}\,(p)\left[-g/b + \left(f_{-\rho}^{-1}\left(\frac{e-p}{a}\right) - \rho g/b\right)\left(f_{-\rho}^{-1}\left(\frac{e-p}{a}\right)\right)^{\delta}\right]\right\}, \qquad (5.5)$$
$$\rho' = \mathrm{sgn}\,(p).$$

The p-dynamics has only a one-step memory since it depends on (the sign of) the immediate preimage only. Anyhow, these results show that in the case of a strong but finite dissipation, when the branched manifold of the extremely dissipative case splits into two, the number of discrete variables specifying the dynamics (either in x or in p) on the manifolds increases by one.

Hénon type maps

We investigate here maps of the class of (2.6) defined, as typically, by a single humped $f(x)$ the maximum of which is chosen to be at $x = 0$. As for the shape of the attractor, the special case of Hénon's map has been extensively studied in the literature [25, 39].

Since the Jacobian J is constant in this class, the quantity $b = -J$ can be considered as the small parameter. As we have seen, in the limit of extremely strong dissipation the shape of the attractor is $x = f(y)$ and the dynamics on it is given by $x' = f(x)$. In first order, y is to be expressed through $x = f(y)$ leading to the dynamics

$$x' = f(x) + b f_{\sigma}^{-1}(x), \qquad (5.6)$$

where f_{σ}^{-1} denotes that branch of f^{-1} where the sign of y is σ. Since $y' = x$, $\sigma' = \mathrm{sgn}\,(x)$. By means of these relations and (5.6) the shape of the attractor immediately follows.

A similar calculation yields in second order the dynamics

$$x' = f(x) + b f_{\sigma}^{-1}(x - b f_{\tau}^{-1}(f_{\sigma}^{-1}(x))), \qquad (5.7)$$

where τ is the sign of the second preimage of x: $\tau' = \sigma$. This shows that inspite of the differences between Lorenz and Hénon type maps the dynamics on branched manifolds is, in both cases, a map of the interval with additional discrete variables, in lowest order the sign of preimages, the number of which increases with the number of branched manifolds. From this point of view there is only a minor difference between

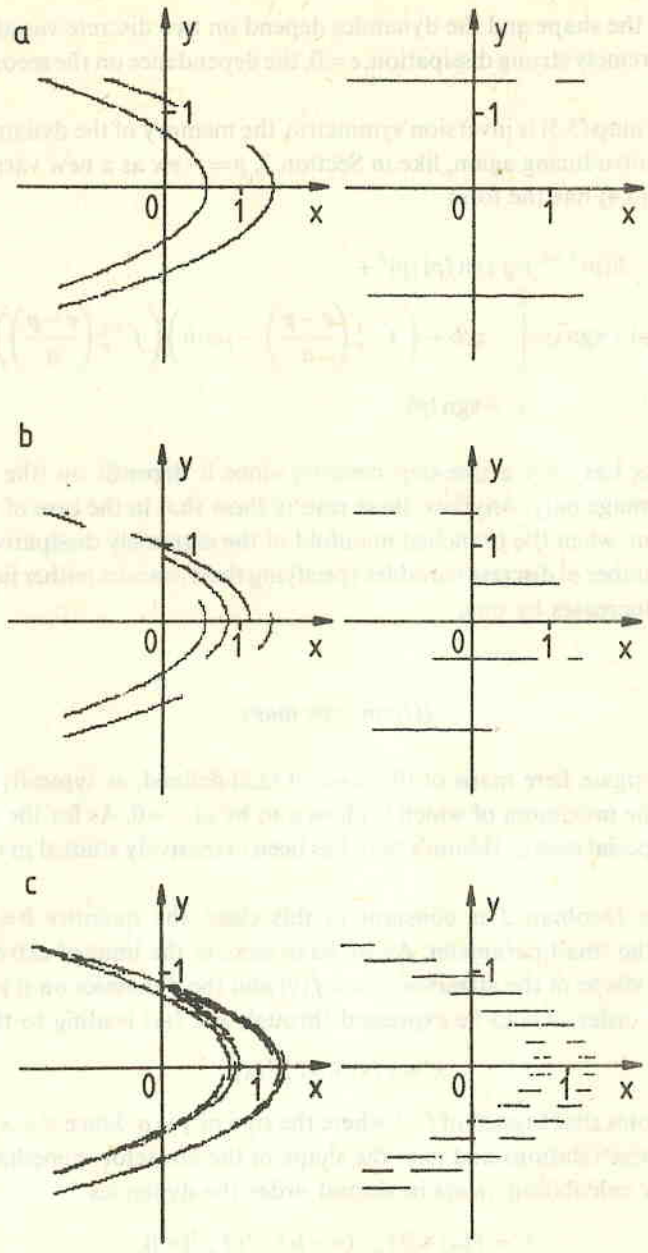
a
y
1
0
1
x
y
1
0
1
x
b
y
1
0
1
x
y
1
0
1
x
c
y
1
0
1
x
y
1
0
1
x

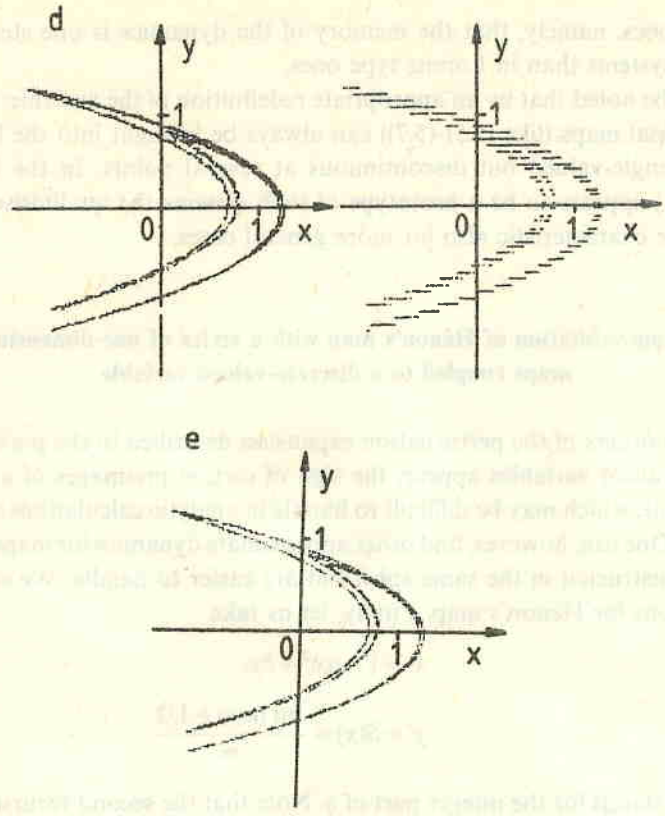

Fig. 8. The chaotic attractor obtained in numerical simulations of (6.1) (shown in the right column) and of (6.2) (left column) at increasing step numbers (m or N) in crisis configuration.
a) $N=2$ ($m=0.35$), $a=a_c=1.068$, $b=0.3$,
b) $N=4$ ($m=1.05$), $a=a_c=1.164$, $b=0.3$,
c) $N=16$ ($m=5.85$), $a=a_c=1.404$, $b=0.3$,
d) $N=38$ ($m=14.45$), $a=a_c=1.413$, $b=0.3$,
e) The Hénon map at $a=a_c=1.427$, $b=0.3$.

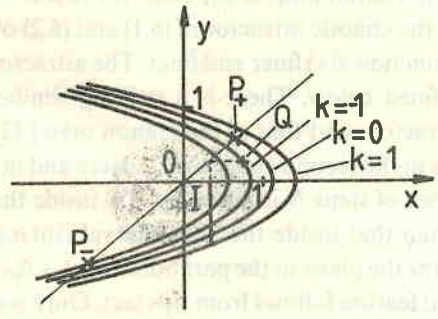

Fig. 9. The parabolas $x=1+b(k+1/2)/m-ay^2$ for $k=-2,-1,0,1$, the preimage I of a point Q, and the fixed points P_+, P_- of (6.2). The parameter values agree with those of Fig. 8b

these two classes, namely, that the memory of the dynamics is one step shorter in Hénon type systems than in Lorenz type ones.

It is to be noted that by an appropriate redefinition of the variable, multivalued one-dimensional maps (like (5.5)–(5.7)) can always be brought into the form of (2.8) where f is single-valued but discontinuous at several points. In the light of this comment (4.1) appears to be a prototype of such systems the qualitative features of which may be characteristic also for more general cases.

6. Approximation of Hénon's map with a series of one-dimensional maps coupled to a discrete-valued variable

In high orders of the perturbation expansion described in the previous Section several two-valued variables appear, the sign of certain preimages of a continuum-valued variable, which may be difficult to handle in analytic calculations or numerical simulations. One can, however, find other approximate dynamics for maps of the plane which are constructed in the same spirit but are easier to handle. We consider here approximations for Hénon's map. Firstly, let us take

$$x' = 1 - ax^2 + by, \tag{6.1a}$$

$$y' = S(x) \equiv \frac{\text{Int}\,(mx) + 1/2}{m}, \tag{6.1b}$$

where Int (q) stands for the integer part of q. Note that the second recursion, $y' = x$, of (2.6) has been replaced by a piecewise constant form (6.1b) with segment length $1/m$. In the following another approximation will be used where the first equation of (2.6) is modified and the second one remains unchanged:

$$x' = 1 - ax^2 + bS(y),$$
$$y' = x. \tag{6.2}$$

An approach toward the Hénon map is expected for $m \gg 1$.

Figure 8 displays the chaotic attractor of (6.1) and (6.2) obtained numerically by making the multi-step function $S(x)$ finer and finer. The attractors are plotted in a crisis configuration to be defined below. There is a striking similarity in the geometrical appearance of these attractors and that of the Hénon map [12] at already rather low step numbers, especially in the second version (6.2). Here and in the following it is more natural to use the number of steps N induced by $S(x)$ inside the maximal extension of the chaotic attractor than that inside the unit interval (Int (m)).

Equation (6.2) maps the plane to the parabolas $x = 1 + b(k + 1/2)/m - ay^2$, where k is an integer. An unusual feature follows from this fact. Only points on these parabolas possess preimages, and such a preimage is a straight line segment (see Fig. 9). Consequently, the chaotic attractor of (6.2) lies on a finite number of parabolas only,

and the dynamics on the attractor is essentially a map of the interval coupled to an extra multi-valued variable.

We have studied in detail the attractors of (6.2) in crisis configuration. Crisis in two-dimensional maps is defined by the existence of heteroclinic tangencies of stable and unstable manifolds [40, 23]. In Hénon's map the crisis when the unstable manifold W^u_+ of the hyperbolic fixed point P_+ touches the stable manifold W^s_- of the hyperbolic fixed point P_-, situated in the negative quadrant, defines a critical line $a=a_c(b)$ in the parameter space. Beyond this line no one-piece chaotic attractor, which is the closure of W^u_+ [40], may exist.

In the map (6.2) there are hyperbolic fixed points analogous with those of the Hénon map. Due to the special multi-step nature of (6.2) the stable manifold W^s_- is discontinuous and consists of straight line segments, which are the preimages of the fixed point P_-. The unstable manifold W^u_+ is also discontinuous and consists of parabola segments. (If there exists a chaotic attractor which contains P_+, it agrees in this case with W^u_+.)

In a certain region of the parameter space these manifolds have no common points (Fig. 10a).

Let w denote the highest index k at which the maximum point of the corresponding parabola still belongs to W^u_+. There are two topologically different possibilities for tangencies between W^u_+ and W^s_-.

Case a: The wth parabola touches W^s_-,

Case b): The endpoint of a segment of W^u_+ (with $k>w$) collides with W^s_-.

It is clear from (6.2) that together with a tangency also intersections appear since the preimages of a point of tangency are segments of straight line. Figure 10b illustrates case a).

Beyond such a special configuration tangencies turn to intersections. Simultaneously, the region from which trajectories escape to infinity (a part of which is displayed in Fig. 10c as shaded area) overlaps with W^u_+. Therefore, a chaotic attractor containing P_+ cannot exist then (and gives way for a chaotic repeller [38]).

Thus, for maps like (6.2) the crisis line $a=a_c(b)$ is to be defined as the borderline of that region of the parameter space where W^u_+ and W^s_- have no common points. The crisis configuration realized at $a=a_c(b)$ is then characterized by a simultaneous appearance of heteroclinic tangencies and intersections but without any escape.

The critical value $a_c(b)$ obtained at a fixed b for increasing step numbers N (which can be expressed in terms of other parameters as $N=2m+1+(2w+1)b$) have been found to approach rapidly the crisis value for the Hénon map at the same b (for data see caption of Fig. 8).

We have determined numerically also the bifurcation diagram along the crisis line at different fixed values of the step number N. Fig. 11 illustrates at $N=8$ that there is an interplay between chaotic and periodic regimes. Thus, in this system crisis is again not a sufficient condition for chaos (not even in a numerical sense).

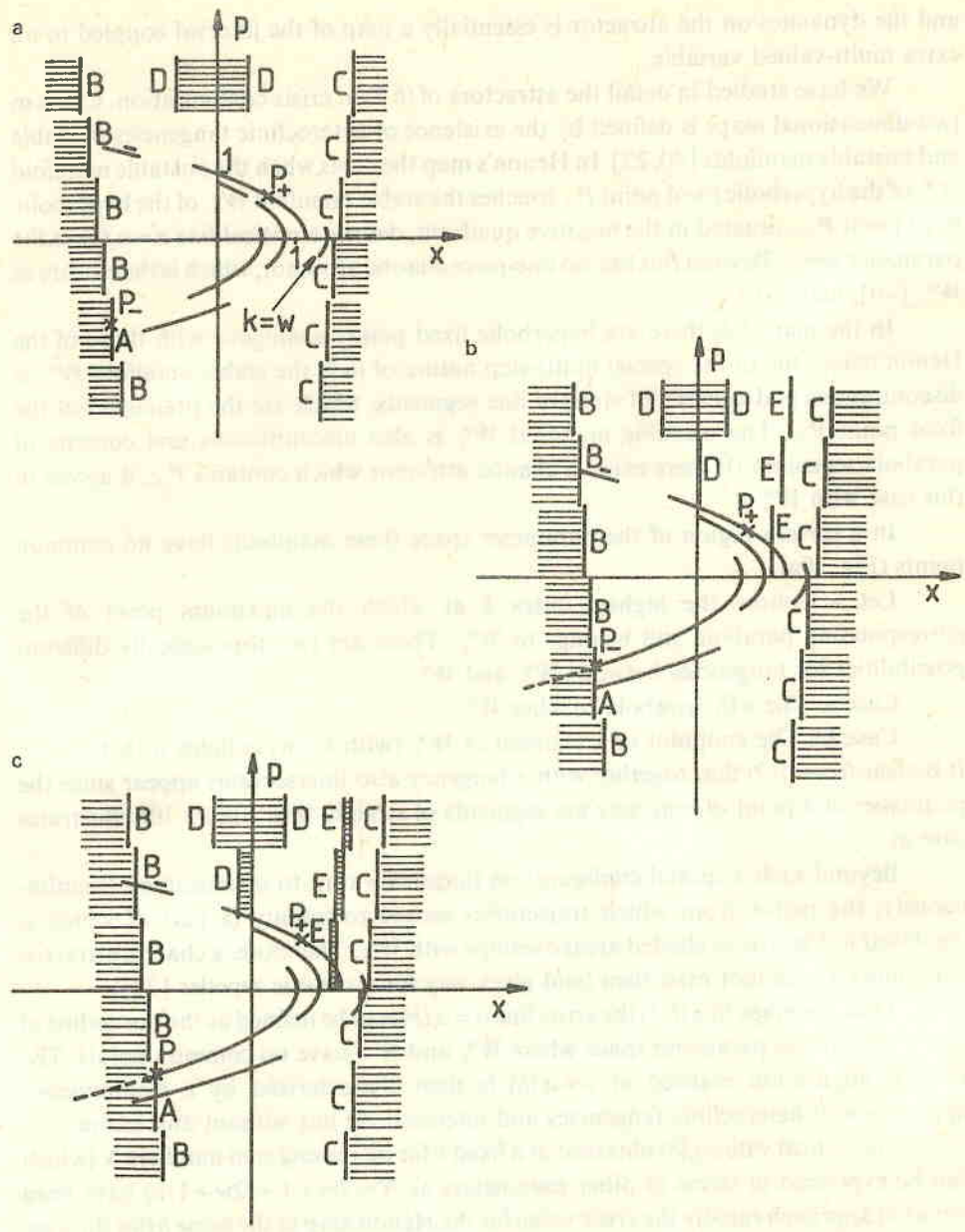

Fig. 10. The unstable manifold W^u_+ (bold line) and a few branches of the stable manifold W^s_- (straight line segments) in (6.2) at different values of a ($b=0.3$). The segment A is the first preimage of P_-, the B-s are its second preimages. Subsequent further preimages are denoted by C, D and E. Trajectories starting from the dashed region are mapped in at most 5 iterations on the parabola arch drawn by a dashed line, where they go to infinity from.

a) $a<a_c=1.164$, no heteroclinic points,

b) $a=a_c$, heteroclinic tangencies and intersections, but no escape from W^u_+,

c) $a>a_c$, escape occurs

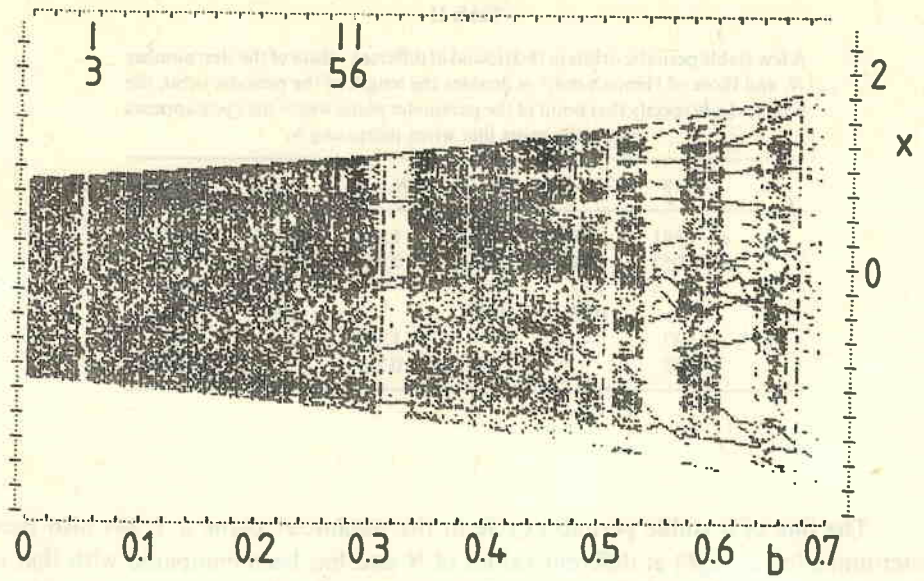

Fig. 11. Bifurcation diagram of (6.2) along its crisis line obtained at a fixed step number $N = 8$. The slashes on the top denote the position of stable 3,5,6-cycles in the Hénon map

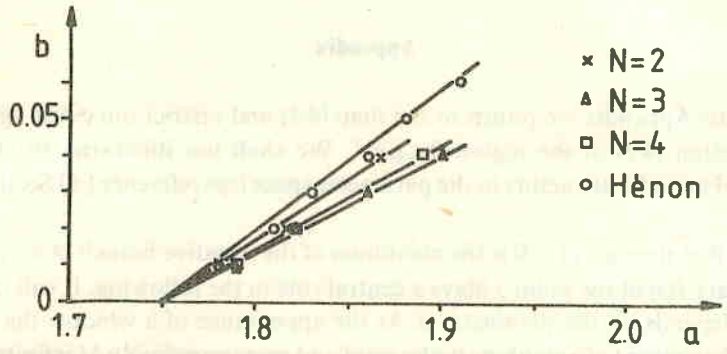

Fig. 12. Position of the stable 3-cycle in the parameter plane a, b for the Hénon map and for (6.2) with step numbers $N = 2, 3, 4$

The position of the largest periodic windows has been specified and compared with that of Hénon's model appearing along its crisis line. It can be seen from Table II that, although not all periodic cycles of the Hénon map can be observed in (6.2) at arbitrary values of N, if a window disappears at a certain N it reappears at a somewhat larger one and the values specifying its position tend toward those of the Hénon map.

Table II

A few stable periodic orbits in (6.2) found at different values of the step number N, and those of Hénon's map. m denotes the length of the periodic orbit, the couples (a, b) specify that point of the parameter plane where the cycle appears along the crisis line when increasing b

m	$N=8$	$N=10$	$N=16$	$N=24$	$N=39$	Hénon
3	$a=1.891$	1.893	1.893	1.895	1.895	1.895
	$b=0.052$	0.047	0.051	0.050	0.051	0.053
5	–	1.50	1.46	–	1.48	1.48
	–	0.23	0.27	–	0.26	0.27
6	1.37	–	–	1.50	–	1.46
	0.32	–	–	0.25	–	0.28

The line of a stable period-3 cycle in the parameter plane a, b has also been determined for $a \leq a_c(b)$ at different values of N and has been compared with that of Hénon's map [41]. Fig. 12 shows a qualitative agreement already at rather small step numbers.

These investigations support the view that the map (6.2) can be a reasonable approximation of Hénon's map for not too weak dissipations.

Appendix

In this Appendix we return to the map (4.1) and restrict ourselves again to the crisis situation (4.2) in the region $0<g<1$. We shall use itineraries to classify the windows of periodic attractors in the parameter space (see reference [6] Section II.1 for definitions).

The first iterate s of -0 is the maximum of the negative branch of h, i.e. $s=1-g$. The itinerary $I(s)$ of the point s plays a central role in the following. It will be denoted by M. It depends on the parameter g. At the appearance of a window the point -0 becomes the element of a stable periodic orbit and correspondingly M is finite: $M=DC$, where D is a finite sequence of R and L symbols. Inside the window the itinerary of s is infinite $M=(DL)^{\infty}$. One can use the repeated sequence $E=DL$ to identify the window.

Let us introduce the ordering between itineraries [6] here. Considering two different itineraries A, B let i be the first index for which $A_i \neq B_i$. Let n denote the number of R's in $A_0 A_1 \ldots A_{i-1}$. By definition $L<C<R$. It is said that $A<B$ if either

a) $A_i<B_i$ and n is even, or

b) $A_i>B_i$ and n is odd.

It is easy to see that the orderings $p \leq q$ and $I(p) \leq I(q)$ are equivalent.

The itinerary of the iterates of a point p can be obtained by shifting the itinerary of p $I(h^n(p)) = \{I_n, I_{n+1}, I_{n+2}, \ldots\}$, which can be written with the help of the shift operator as

$$I(h^n(p)) = S^n I(p). \tag{A.1}$$

For any itinerary we obtain $I(h^n(p)) < I(-0) \equiv LM$ if $h^n(p) < 0$, thus

$$S^{n+1} I(p) < M \qquad \text{for} \quad I_n = L. \tag{A.2}$$

For $p = s$ it gives

$$S^{n+1} M < M \qquad \text{for} \quad M_n = L. \tag{A.3}$$

The itinerary M plays a similar role in these conditions as the kneeding sequence for unimodal maps [6].

In the following we restrict ourselves to the case when the separate intervals I_1, I_2, I_3 are mapped into each other according to (4.3) (see Fig. 7). It is fulfilled in the region $g_3 < g < 1$. It can be easily seen that R's inside the itineraries may occur only in RR pairs followed by L. So itineraries of points in I_2 can be written as a product

$$I = N_{l_1} N_{l_2} \ldots N_{l_n} C \qquad \text{or} \quad I = N_{l_1} N_{l_2} \ldots,$$

where

$$N_l = R^2 L^l, \qquad l, l_i > 0.$$

Correspondingly, the itinerary M has this form. The situation when M is finite corresponds to the appearance of a window, the repeated sequence belonging to the stable periodic orbit in the window is

$$E = DL = N_{k_1} N_{k_2} \ldots N_{k_n}, \qquad k_i > 0. \tag{A.4}$$

The allowed sequence $\{k_i\}_{i=1}^n$ of the subscripts is selected by the requirement (A.3) for $M = DC$.

On the basis of this description we get for the windows investigated in Section 4

$$E_m = N_{m-2} = R^2 L^{m-2}, \qquad m > 2 \tag{A.5}$$

and we find satellite series of windows

$$E_{m,-k} = N_{m-3} N_{m-3+k}, \qquad m > 3, \quad k > 0,$$

$$E_{m,k} = (N_{m-2})^k L = (N_{m-2})^{k-1} N_{m-1}, \qquad m2 > 2, \quad k > 1.$$

The parameter values of $E_{m,-k}(E_{m,k})$ tend to the $g_m^<(g_m^>)$ value where the stable period E_m appears (disappears). Some of these windows were observed in bifurcation diagrams.

References

1. R. H. G. Helleman, in Fundamental Problems in Statistical Mechanics, Vol. 5, ed. E. G. D. Cohen, North Holland, Amsterdam, 1980.
2. A. J. Lichtenberg and M. A. Lieberman, Regular and Stochastic Motion, Springer, N. Y., 1983.
3. H. G. Schuster, Deterministic Chaos, VHC Publishers, Weinheim, 1984.
4. H. Poincaré, Les méthodes nouvelles de la mécanique céleste, Gauthier Villars, Paris, 1892.
5. M. Misiurewicz, Maps of an interval, in: Chaotic Behaviour of Deterministic Systems, ed. G. Ioos, R. H. G. Helleman and R. Stora, North-Holland, Amsterdam, 1983.
6. P. Collet and J.-P. Eckmann, Iterated Maps on the Interval as Dynamical Systems, Birkhäuser, Boston, 1980.
7. B. V. Chirikov, Phys. Reports, *52*, 263, 1979.
8. J.-P. Eckmann and D. Ruelle, Rev. Mod. Phys., *57*, 617, 1985.
9. B. Mandelbrot, The Fractal Geometry of Nature, Freeman, San Francisco, 1982.
10. O. E. Rössler, Phys. Lett., *57A*, 397, 1976.
11. M. Hénon and Y. Pomeau, Lecture Notes in Math., *565*, 29, 1976.
12. M. Hénon, Commun. Math. Phys., *50*, 69, 1976.
13. E. N. Lorenz, J. Atmospheric Sci., *20*, 130, 167, 1963.
14. T. Rikitake, Proc. Cambridge Phil. Soc., *54*, 89, 1958.
15. O. E. Rössler, Z. Naturforsch., *31a*, 1664, 1976.
16. R. F. Williams, Lecture Notes in Math., *615*, 94, 1977.
17. J. A. Yorke and E. D. Yorke, J. Stat. Phys., *21*, 263, 1979.
18. A. Arneodo, P. Coullet and C. Tresser, Phys. Lett., *81A*, 197, 1981.
19. C. Sparrow, The Lorenz Equation: Bifurcations, Chaos and Strange Attractors, Appl. Math. Sci., *41*, Springer, N. Y. 1982.
20. D. V. Lyubimov and M. A. Zaks, Physica, *9D*, 52, 1983.
21. P. Szépfalusy and T. Tél, Physica, *16D*, 252, 1985.
22. G. Györgyi and P. Szépfalusy, J. Stat. Phys., *34*, 451, 1984.
23. C. Grebogi, E. Ott and J. A. Yorke, Physica, *7D*, 181, 1983.
24. L. Hitzl, Physica, *2D*, 370, 1981.
25. R. Bridges and G. Rowlands, Phys. Lett., *63A*, 189, 1977.
26. R. Lozi, J. de Physique, Colloque *39*, C5, 9, 1978.
27. J. P. Crutchfield, D. Farmer, N. Packard, R. Shaw, G. Jones, R. J. Donnely, Phys. Lett., *76A*, 1, 1980.
28. R. B. May, Nature, *261*, 459, 1976.
29. S. Grossmann and S. Thomae, Z. Naturforsch., *32a*, 1353, 1977.
30. M. J. Feigenbaum, J. Stat. Phys., *19*, 25, 1978; *21*, 669, 1979.
31. T. Geisel and J. Nierwetberg, Phys. Rev. Lett., *47*, 975, 1981.
32. L. P. Shilnikov, Math. USSR Sbornik, *6*, 427, 1968.
33. P. Gaspard, Phys. Lett., *97A*, 1, 1983.
34. P. Glendinning and C. Sparrow, J. Stat. Phys., *35*, 645, 1984.
35. P. Gaspard, R. Kapral and G. Nicolis, J. Stat. Phys., *35*, 697, 1984.
36. A. Arneodo, P. H. Coullet, E. A. Spiegel and C. Tresser, Physica, *14D*, 327, 1985.
37. O. E. Lanford, Limit Theorems in Statistical Mechanics, Troisième Cycle de la Physique, E. N. Suisse Romande, Semestre d'Eté, 1978.
38. H. Kantz and P. Grassberger, Physica, *17D*, 75, 1985.
39. H. Daido, Prog. Theor. Phys., *63*, 1190, 1980.
40. C. Simo, J. Stat. Phys., *21*, 465, 1979.
41. D. L. Hitzl and F. Zele, Physica, *14D*, 305, 1985.